

Characteristics of liquid water transport and corner effect in microfluidic channels of PEM fuel cell

Donghao Ye^{1,2}, Liuli Zeng^{2,3}, Wei Guo^{2,3,*}

¹ Wuhan Marine Electric Propulsion Research Institute, Nanhu Qixiao, Wuhan, China 430064

² State Key Laboratory of Advanced Technology for Materials Synthesis and Processing, Wuhan University of Technology, Luoshi Road 122#, Wuhan 430070, PR China

³ Foshan Xianhu Laboratory of the Advanced Energy Science and Technology Guangdong Laboratory, Xianhu Hydrogen

*E-mail: guowei2016@whut.edu.cn

Received: 14 June 2022 / Accepted: 5 August 2022 / Published: 10 October 2022

The water generated in the catalyst layer flows through the GDL (gas diffusion layer) and passes through the microfluidic channels of fuel cells. In this study, characteristics of water motion in the microfluidic channels are investigated corresponding to various Reynolds numbers and compression ratios of GDL. Gas can bypass the rib to the adjacent channel and flows through the GDL underneath the slug. To remove the slug, the bypass distance (%) and gas flow rate should be larger than 13%. The cross-section shape of the slug in 1-wall hydrophobic GDL and 3-walls hydrophilic acrylic channel is an analogous upside-down trapezoid. Since the required GDL compression ratio should be over 13% to eliminate liquid water instead of simply increasing the volumetric gas flow, the residual droplets are received at the vertical corner in the channel, compared to the arc corner. The regimes of liquid water flow in the 1-wall hydrophobic GDL and 3-walls hydrophilic acrylic channel are summarized as slug motion, compressed drop motion, elongate droplet motion, drop oscillation, and cap drop motion. These results provide improved physical models predicting the state of water hold-up and flooding in PEM fuel cells.

Keywords: Microfluidic channel; Arc/vertical turning; GDL; Gas flow rates; Fuel cell

1. INTRODUCTION

The environmental, economic, and sustainable implications demand a dwindling supply of fossil fuels due to increasing energy demands. Proton exchange membrane (PEM) fuel cells are clean energy devices utilizing hydrogen and oxygen to generate power. Water is the only effluent of this energy conversion device. Therefore, water management in these devices is the biggest challenge for fuel cell engineers in their broader implementation. Singh, Rupinder. [1] reviewed the degradation aspects of

water formation and transport in PEM fuel cells suggesting that the water management system affected PEM fuel cell performance and durability.

Water is generated in the cathode layer, passes through the GDL via lateral flow and transverse flow, and arrives at the channel. Kalidindi, A. R. [2] developed a two-phase model studying the role of interfacial voids at the microporous layer and catalyst layer interface on PEM fuel cell performance. Their findings revealed that the liquid water saturation in interfacial voids was significantly affected by their geometry and location. Luo, F. [3] studied the water transport characteristics of a PEM fuel cell at different operating pressures and temperatures, managing water with saturated hydrogen and dry air. There was no water transport from the cathode to the anode. B. H. Lim. [4] investigated that the concentrations of water at the anode and cathode were the same at a relative humidity of 58% and 20%, respectively. Moreover, no diffusion of water occurred in the PEM fuel cell under these conditions. Zago, M. [5] studied the water flow in, through, and around the GDL. The water flow resistance was approximately ten times larger than the resistance to water flow between a GDL surface and a smooth solid surface. Polverino's group [6-9] described a single droplet deformation, oscillation, and detachment on the GDL surface. A dynamic force balance was implemented considering the effects of droplet elastic deformation. Penga, Željko. [10] studied the effects of GDL structure on liquid water management in PEM fuel cells. Water slugs formed, spanning the micro-channel, caused large fluctuations in the local current density. Kristopher Inman. [11] confirmed the slug motion in the serpentine channel, employing a direct experimental visualization in an operational transparent single-serpentine PEM fuel cell. Experimental studies via lab-on-a-chip and microchannel cooling applications revealed two-phase flow patterns in channels [12-16]. Additionally, Djilali's group [17-20] and Benziger's group [21-23] developed microfluidic channels and pressure transducers to study droplet emerging to slug motion in microfluidic channels. The pressure traces corresponding to the liquid motion were very helpful in understanding the processes.

Herein, microfluidic channels with two kinds of turnings are employed to investigate the liquid water transition and the corner effect characteristics. This approach is analogous to serpentine channels in PEM fuel cells. The regimes of liquid water motion in serpentine channels are various due to different gas flow rates (Reynolds number, $2 < Re_{gas} < 600$) and assembled pressures. We also quantized the impact of GDL compressions on the liquid water motion, the effect of Reynolds numbers on liquid flow, and the impact of channel corners on liquid flow.

2. EXPERIMENTAL

Two microfluidic channels with arc turning and vertical turning were employed to investigate the liquid water flow at different gas flow rates and GDL compression ratios. The cross-section of the channel was $1.6 \times 1.6 \text{ mm}^2$, the distance from the water inlet to the turning was 60mm, and the distance from the gas inlet to the water inlet was 11.3mm (Fig. 1). Toray carbon paper (TGP-H-120) with 20% Teflon loading was affixed to the bottom of the acrylic channel with a thin film of silicon grease. The two channels, referred to as the flow channels were prepared with 0.1mm pores through the acrylic block and carbon paper.

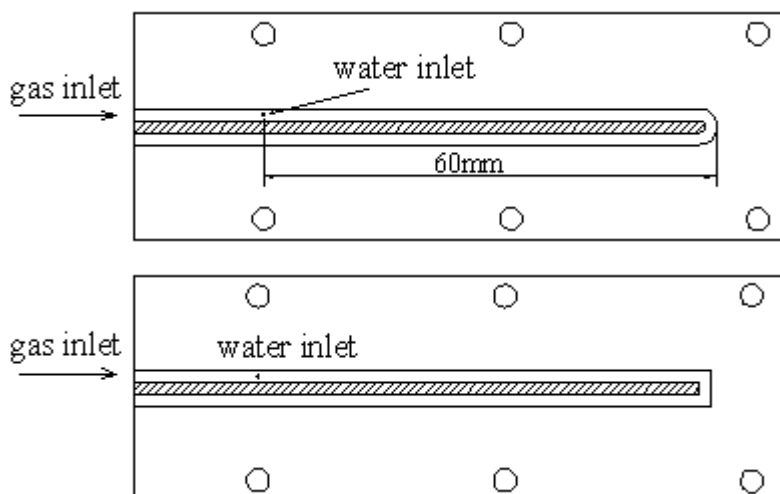


Figure 1. The schematic of the experiment.

In all experiments, water was supplied to the flow channel using a syringe pump at a flow rate of 10 $\mu\text{L}/\text{min}$ while nitrogen gas was passed using a mass flow controller at flow rates ranging from 3–900 mL/min. Different compression levels of GDL were controlled by commercial PTFE sheets of different thicknesses. Thin sheets were incompressible in these experiments.

A low-pressure transducer (Omega PX-160) was employed to acquire the differential pressure between the channel inlet pressure and outlet pressure, $\Delta P = P_{in} - P_{out}$. The measurement range of the pressure transducer was 0–500 (gauge) Pa, with an accuracy of ± 5 Pa. The differential pressure was set at a frequency of 20 Hz. Videos of liquid water motion were captured using a high-speed camera (Phantom V5, Vision Research Inc.). In the experiments, the mass flow rate in the gas flow channel was kept constant. The experimental conditions and physical parameters were summarized in Table S1. The gas flow rates of 3-900mL/min correspond to the gas Reynolds numbers:

$$Re_{gas} = \frac{\rho_{gas} Q_{gas} D_h}{\mu A_{channel}} \quad (1)$$

where Q_{gas} is volumetric gas flow, ρ is gas density, $A_{channel}$ is channel cross-sectional area, D_h is hydraulic diameter, and μ is gas viscosity. The range of the Reynolds number is from 2 – 600.

Wetting properties such as interfacial forces, contact angle hysteresis of the acrylic material in the micro-fluidic cells, and static (advancing/receding) contact angles were determined by Wilhelmy Plate measurements. The acrylic sheet showed advancing and receding contact angles of 84° and 55° while that of the GDL sample were 120° and 70° , respectively.

The rate of water production is given by equation 2 and the airflow exiting the cathode gas flow channel is given by equation 3;

$$\dot{Q}_{water} = \frac{i A M_{water}}{2 F \rho_{water}} \quad (2)$$

$$\dot{Q}_{air} = \frac{i A R T}{4 F P O_2} (\lambda - 1) \quad (3)$$

where i is the current density, A is the active area (equivalent area in the microfluidic cell was 3.8 cm^2), F is Faraday’s constant, M_{water} is the molecular weight of water, ρ_{water} is the density of water, R is the gas constant, T is the temperature, P_{O_2} are the partial pressure of oxygen and λ is the stoichiometric ratio of oxygen in the feed to the oxygen consumed in the reaction. The volumetric water flow was $10 \text{ }\mu\text{L}/\text{min}$ corresponding to a current density of $0.8 \text{ A}/\text{cm}^2$. We fixed the volumetric water flow to investigate the impact of GDL compression ratios and Reynolds number on liquid water flow in microfluidic channels.

3. RESULT AND DISCUSSION

3.1. Effects of compression ratios of GDL on liquid water shedding

GDLs are compressed in PEM fuel cells. Numerous studies focused on the effects of GDLs compression on fuel cell performance [24-31]. However, no definite compression ratio of GDL is reported. The optimal compression ratio of GDL is associated with different factors, such as the combination of material elements, flow field structure, assembly patterns, and operating conditions. In the present study, several compression ratios of GDLs from 13% to 30% are optimized to investigate the characteristic of liquid water flow in the serpentine channel at different Reynolds numbers (Table 1).

Table 1. Liquid water motion at various Reynolds number and GDL compression ratios

GDL compression ratios	Critical Q_{gas} for single slug	Critical Q_{gas} for continuous slugs	Reynolds number	Liquid water regime
13% compression ratio	24	28	$Re_g \leq 33$	① Slug
			$33 < Re_g \leq 66$	① Slug
			$66 < Re_g \leq 200$	③ Compressed drop → slug
			$20 < Re_g < 600$	④ Drop
20% compression ratio	12	14	$Re_g \leq 33$	① Slug
			$33 < Re_g \leq 66$	② Slug
			$66 < Re_g < 200$	③ Compressed drop → slug
			$20 < Re_g < 600$	④ Drop
24% compression ratio	10	12	$Re_g \leq 33$	① Slug
			$33 < Re_g \leq 66$	⑤ Slug and oscillation
			$66 < Re_g \leq 200$	⑥ Compressed big drop
			$20 < Re_g < 600$	④ Drop
30% compression ratio	5	6	$Re_g \leq 33$	① Slug
			$33 < Re_g \leq 66$	⑦ Elongate slug
			$66 < Re_g \leq 200$	⑧ Upside-down droplet → slug
			$200 < Re_g < 600$	④ Drop

① Drop grows into a slug. Slug blocks the channel and moves out. Residual liquid exists in the quarter corner, not in the arc corner.

② Slugs move at high speed, self-detaching after turning in the quarter corner and forming residual liquid hanging on channel walls, unsuitable for the channel with the arc corner.

③ The cap dropping at the water inlet is pushed downstream, forming a long droplet. The droplet finally forms a slug and moves out. The slug stretches and the rear part detaches as residual liquid drop stays in the channel.

④ The cap drops at the water inlet are pushed downstream of the channel and several cap drops form a big droplet moving out.

⑤ Drop grows and forms a pre-slug which oscillates downstream of the water inlet. The volume of the slug is bigger than the slug in the case of ① due to the oscillation.

⑥ A droplet is pushed downstream of the water inlet and forms a long droplet. The gas bypasses the droplet by oscillation. The droplet is big enough and moves out without slug formation.

⑦ The slug is elongated by the gas. The slugs are then transferred to droplets hanging on the top hydrophilic wall of the acrylic channel, reforming a slug again by drawing back or the other liquid drop/slug joining in.

⑧ The cap drop is pushed downstream of the channel and gathers to form an upside-down droplet. The droplet hangs on the top wall of the channel. A big droplet moves out which is stretched and the rear part is detached.

In both 1-wall hydrophobic GDL and 3-walls hydrophilic acrylic channels, gas can bypass the rib through the GDL to adjacent channels. There are critical (lowest) gas flow rates for liquid water elimination from the channel, as summarized in Table 1. The gas flow rate in each channel is larger than the critical values. Based on equation 2, when $\lambda = 2$ the volumetric nitrogen flow is approximately 20mL/min, the corresponding compression ratio of GDL should be 20% to eliminate the slug in the channel. With the increase in compression ratios, the patterns of liquid in the channel are different even at the same Reynolds number. The differences are noted from ① to ⑧ and images are shown in Fig. S1. The slug and drop regimes are shown in the following figures.

At the same Reynolds number, the characteristics of liquid water flow are different, as described in ③ and ⑥ (Fig. S1). The liquid water is elongated by the gas pushing. However, slug motion is at 13% compression of GDL while droplet flows at 24% compression. The permeability of GDL under the rib decreases with increasing compression. Less volumetric gas flows through the GDL when the rib promotes liquid water compression and drop flow formation. Increasing GDL compression is an alternative to increasing the gas flow rates to eliminate liquid water in the channel[32]. With the increase in Reynolds number, the liquid flow characteristics in the microfluidic channel are analyzed below. The compression ratio of GDL is 24% at this point.

3.2 Droplet evolution in a square channel with different wettabilities.

Colosqui [33] investigated the droplet and slug formation in the 4-walls hydrophilic channel. The water initially formed a spherical cap anchored in the pore. Fig. 2 shows that the water coming out of the biggest pore in the GDL forms a cap. In the 4-walls hydrophobic channel, the droplet grows and

spans the channel from side to side without touching the wall opposite to the emergent pore. The laterally confined droplet first touches the wall at the channel corner and a gap is formed between the droplet and the opposite wall to allow the gas flow [34]. The droplet then spans the channel, forming a slug. However, in 3 hydrophilic walls and 1 hydrophobic GDL wall, the droplet continues to grow and randomly touches one side wall after forming a spherical cap (Fig. 2b). The droplet kept grows along the side wall, touches the top wall, and then arrives at another side wall when the gas and water fed in, (Fig. 2b-2d). The path is either anticlockwise or clockwise. The contact area on the GDL is much smaller than that on the acrylic surface. The area with the deeper color, shown in Fig. 2 (top view), is the contact area between the droplet and the GDL surface. The lighter color indicates the contact area between the droplet and the acrylic surface. Owing to the different wettabilities, an upside-down trapezoid is formed when the slug moves along the channel.

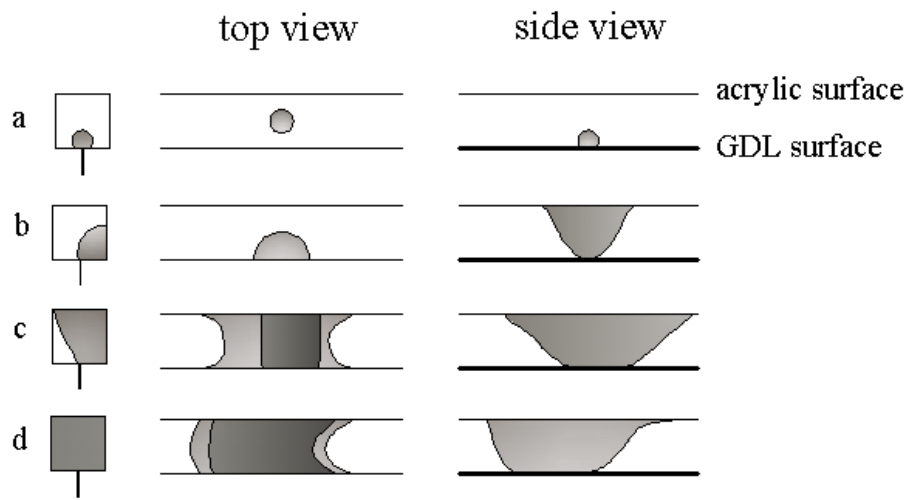


Figure 2. Schematic illustration of the drop evolution in a square channel (1-wall GDL and 3-walls).

3.3 Single slug motion under low gas flow rates (<10mL/min) in serpentine channel

Fig. 3 shows the single slug motion in the channel with a vertical corner when the Re_{gas} was $2 < Re_{gas} < 7$ flow regime. Based on the size of flow channels, flow rates correspond to fuel cell operation with current densities $<500\text{mA}/\text{cm}^2$ [34] and the air stoichiometry at the cathode is around 2. The gas primarily bypasses the rib and moves out instead of pushing the slug moving. The detachment pressure ($P_{detachment}$) is fixed, depending on the wettability of the channel. The slug moves as long as the bypass pressure (P_{bypass}) increases than the $P_{detachment}$. The slug stops when the $P_{bypass} = P_{detachment}$, as shown in equation 4:

$$3(\cos \theta_{R,acrylic} - \cos \theta_{A,acrylic}) + (\cos \theta_{R,GDL} - \cos \theta_{A,GDL}) = \frac{\mu_{gas} w^2}{\gamma_w k_{GDL} t_{GDL}} \frac{Q_{gas}}{D_{bypass}} \quad (4)$$

where γ_w is the surface tension of water, and θ_R and θ_A are receding and advancing contact angles of water with GDL and acrylic surfaces. The channel is square (1.6mm*1.6mm), and w is the width and depth of the channel. Q_{gas} is the gas flow rate, k_{GDL} is the GDL permeability, μ_{gas} is the viscosity of the gas, w_{rib} is the width of the rib, t_{GDL} is the GDL thickness, and D_{bypass} is the bypassing distance from the water inlet to the tail of the slug.

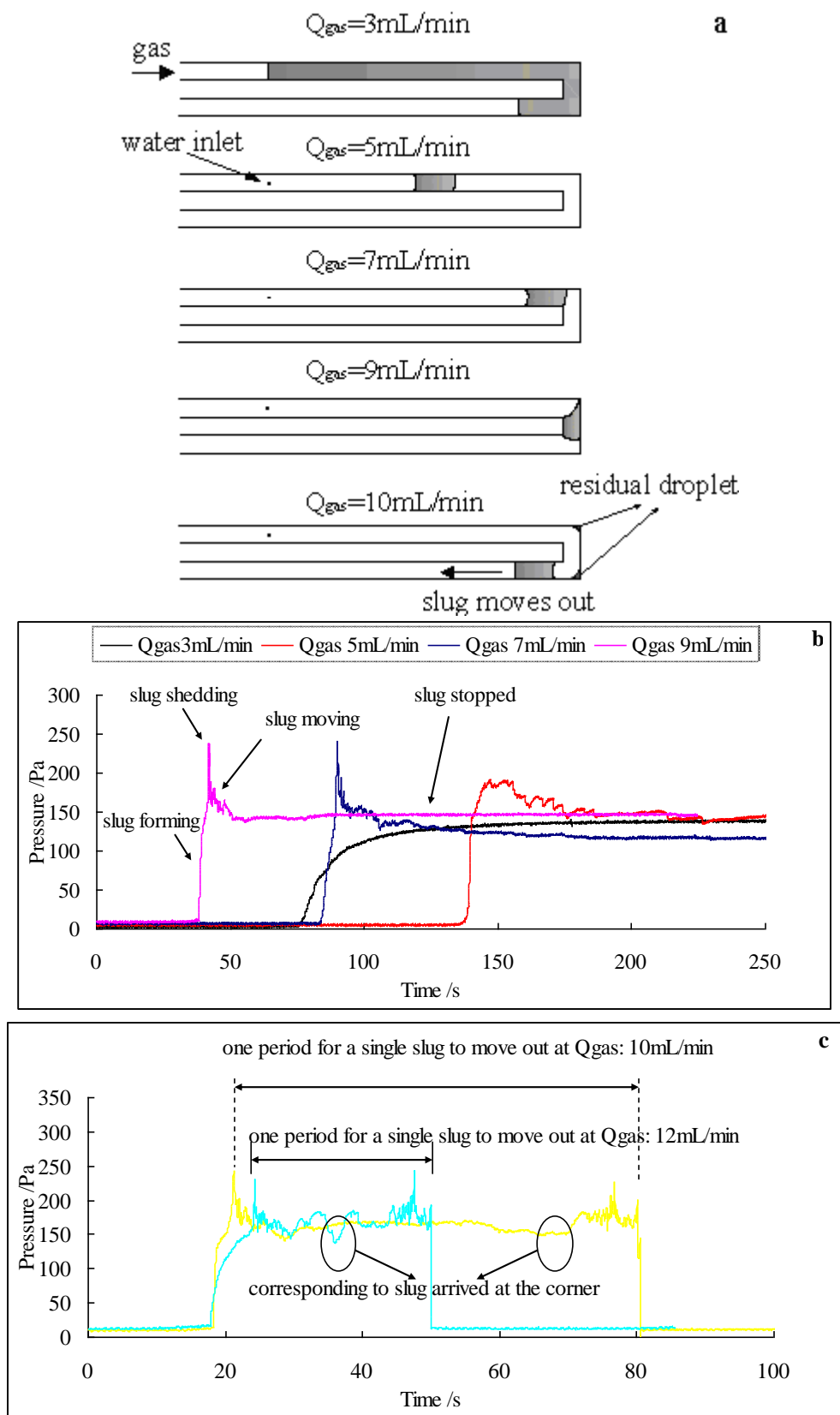


Figure 3. Single slug motion at different flow rates in the vertical corner channel. The water flow rate of $10\mu\text{L}/\text{min}$ and $Q_{gas} = 10\text{mL}/\text{min}$ is the critical value for a single slug to move out. a) The images of slug motion in the channel, and (b and c) the pressure traces corresponding to the slug motion.

Fig. 3 displays a single slug motion for $0 < Re_g < 7$ in the microchannel with turning. The slug motion is shown in Fig. 3a. The slug stops at different locations in the channel, corresponding to different gas flow rates. The pressure traces (Fig. 3b) corresponds to the single slug motion in Fig. 3a. The critical value of the gas flow rate is 10mL/min ($Re_g = 7$) for a single slug moving out. For $Re_g \leq 2$, liquid water comes out of the biggest pore and forms a long liquid column. The gas bypasses the rib to the adjacent channel through the GDL at this compression ratio. The long liquid column moves out after filling the channel. The $P_{detachment}$ is much lower than the P_{bypass} . For $2 < Re_g < 6$, the liquid water comes out of the GDL and forms a slug. The slug moves and the P_{bypass} decreases with increasing D_b . The slug stops at $P_{bypass} = P_{detachment}$, as shown in equation 4. The process of one slug motion in the channel is marked in the pink curve (Fig. 3b). Here, the P_{bypass} is 120Pa and the $P_{detachment}$ is approximately 160Pa. For $Re_g \geq 7$, the lowest P_{bypass} for the slug reaching the corner is still higher than the $P_{detachment}$. $Re_g = 7$ indicates $P_{bypass} = P_{detachment}$. The critical time for a slug to move out is approximately 60s, approximately 2 times longer than the time just $Re_g = 8$ (Fig. 3c). There is the lowest point in the pressure trace, marked in Fig. 3c, corresponding to the slug arriving at the corner in the channel.

According to equation 2, Q_{gas}/D_{bypass} should remain constant, as indicated in Fig. S2. The experimental data results are consistent with the prediction in Equation 4. Moreover, the Q_{gas}/D_{bypass} should be at least 0.13 to eliminate the accumulated water in the channel.

Fig. S3 displays the characteristic of slug passing through the quarter corner and arc corner. The shape of the slug in the arc corner is the same as moving in the straight channel. In addition, the arc corner has little impact on the slug motion. However, slug motion in the quarter corner is different from that in the arc corner. The head of the slug shows an inertial motion instead of adjusting the corner (Fig. S3). The abrupt turning of the quarter corner changes the liquid-solid interfacial energy (γ_{ls}) to liquid-vapor interfacial energy (γ_{lg}). The interfacial energy for the slug is the sum of the liquid-vapor and liquid-solid energies as shown in equation 5;

$$\gamma_{sg} = \gamma \cos \theta_{lg} \quad (5)$$

The liquid-vapor interfacial energy is higher than the solid-liquid interfacial energy, holding the slug and preventing liquid touch the solid wall. The directions of slug motion and gas flow in the arc corner and quarter corner are marked in Fig. S3. There is a residual liquid at the vertical turning off the channel (Fig. 3a and S3). However, the smooth arc turning pattern eliminates all residue at the corner of the channel, the main difference between the channel with vertical turning and the channel with arc turning. Those residual liquids act as nucleating sites for subsequent drop-to-slug transitions. When the slug is pushed down the channel, another residual micro-droplet is left behind at approximately the same location [35].

3.4 Continuous slugs motion under low gas flow rates (<12mL/min) in the serpentine channel

Continuous slug motion in the micro-fluidic channel is shown in Fig. S4. The gas and water flow rates are 9mL/min and 10 μ L/min, respectively. There are 6 evolutions in one period (Fig. S4). When the second slug is formed and moves, the first slug stops. The gas pushes the second slug instead of pushing

the first slug. Therefore, when a new slug is formed and blocks the channel, the previous slugs stop moving. However, the gap between the two slugs reduces, as shown in evolution 4 and 5. As shown in Fig. S4 (evolution 6), the previous slugs are combined as one long slug, contributing to one period, and then returning to evolution 2. The slugs unite into one and move out of the channel before a new slug formation.

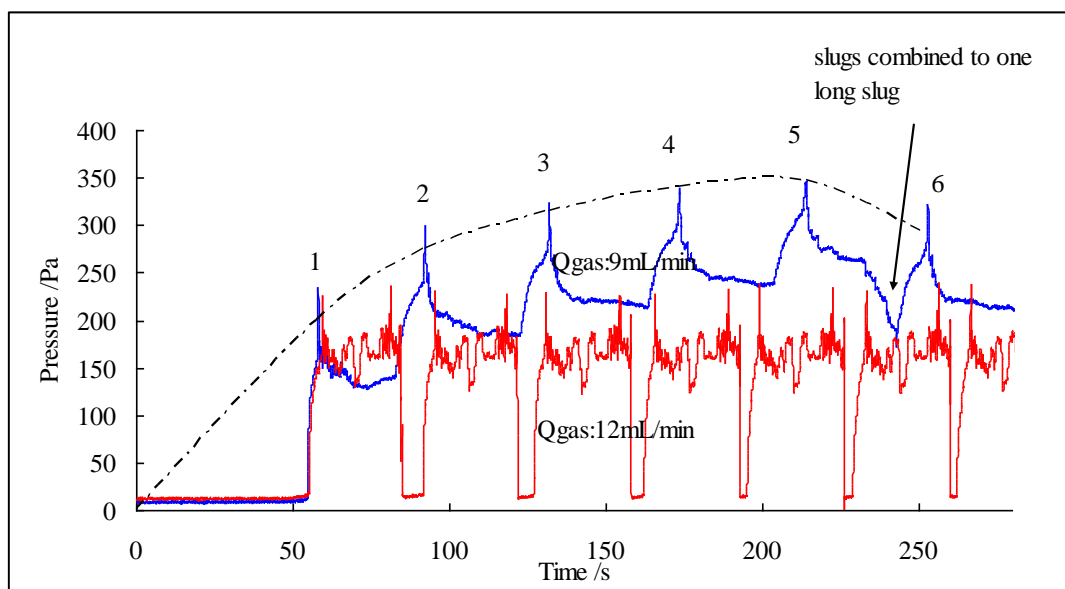


Figure 4. Gas pressures as a function of time for continuous slugs motion in the channel with a vertical corner. $Q_{gas} = 12\text{mL}/\text{min}$ is the minimum value for slugs to move out when the water flow rate was $10\mu\text{L}/\text{min}$.

Fig. 4 shows the gas pressure trace corresponding to the slug motion. The critical gas and water flow rate flow rates are $12\text{mL}/\text{min}$ and $10\mu\text{L}/\text{min}$, respectively. The pressure trace for one slug motion period is like an “M”. The sinus point in the “M” indicates that the slug reaches the corner in the channel the highest D_{bypass} and the lowest P_{bypass} . When the gas flow rates are lower than $12\text{mL}/\text{min}$, the slugs motion characters are shown in Fig. S4 and one pressure trace of $9\text{mL}/\text{min}$ is shown in Fig. 4. The numbers in Fig. 4 correspond to the numbers in Fig. S4. The pressure increases with the number of slugs in the channel. When the slugs are combined into one, the pressure decreases. The pressure in evolution 6 is almost equal to the pressure in evolution 4. Gas has three ways to move ahead: push the slug, go through the GDL underneath the slug and bypass the rib. In this study, bypassing the rib is the preferable route for gas to move forward. The increasing pressure is attributed to the gas passing through the GDL underneath slugs.

3.5 Liquid motion in high gas flow rates in the serpentine channel

Oscillation of the droplet occurs at the water inlet before forming a slug when $Re_{gas} > 36$ (Fig. 5). The side views of the droplet oscillation and videos are available at

http://pemfc.princeton.edu/MFC_Data. Polverino [6] developed a numerical model of the droplet growing on the GDL surface. The droplets oscillation has a complex dynamic interaction among the surface tension force, drag force, and inertial force.

$$3\gamma_w w (\cos \theta_{R,acrylic} - \cos \theta_{A,acrylic}) + \gamma_w w (\cos \theta_{R,GDL} - \cos \theta_{A,GDL}) = \frac{1}{2} \rho_{gas} Q_{gas}^2 C_D E_d + m \frac{dl^2}{dt^2} \quad (5)$$

where $\frac{1}{2} \rho_{gas} Q_{gas}^2 C_D E_d$ is the drag force, C_D is the drag coefficient, $E_d = R^2 \left[\theta_s - \frac{\sin(2\theta_s)}{2} \right]$ is the droplet cross-sectional area for the gas flow, and θ_s is the basic contact angle depending on material properties. $m \frac{dl^2}{dt^2}$ is the inertial force and m corresponds to the droplet mass.

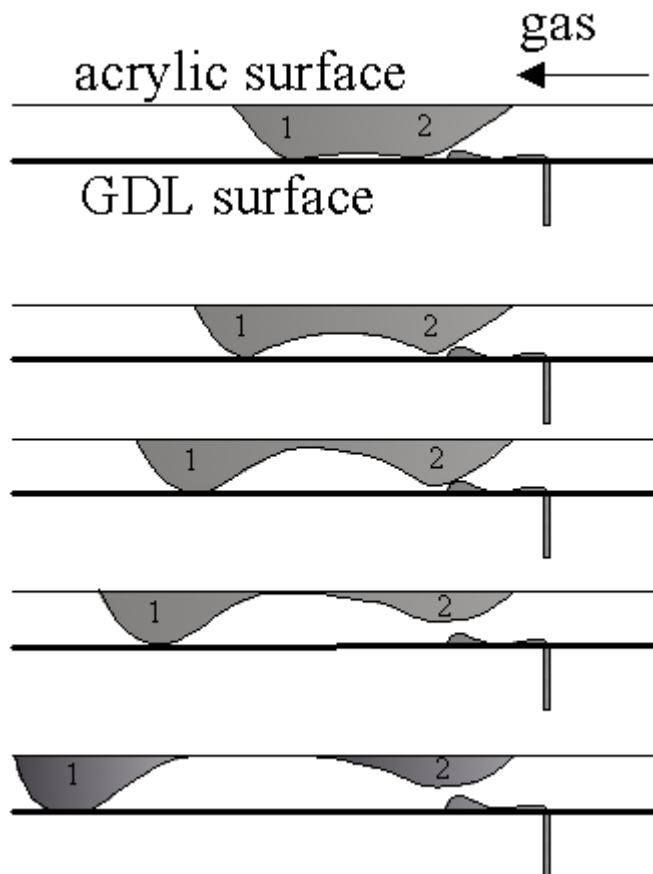


Figure 5. Side view of the slug formation at high gas flow rates (50-300mL/min) in the channel with a vertical corner. At a water flow rate of 10 μ L/min, droplet oscillation can be detected.

Due to gas thrusting, the location of droplet formation is a little ahead of the inlet pore (Fig. 5). There are two parts of the droplet before slug formation. Part 2 acts as a substantial liquid provider of part 1 and the separation of the two parts increases due to the droplet oscillation. Part 1 finally forms a slug and moves out and part 2 is a residual droplet near the water inlet. The oscillation processes are similar to the drag force exerting a thrust on an exposed droplet surface, with a subsequent deformation. The surface tension responds to this deformation by bringing the droplet back to its original shape [36] (i.e. the surface tension reduces the energy content of droplet surface molecules).

Fig. S5 shows the in-situ pressure of droplet oscillation and slug motion. The period shown in Fig. S5 is 44s while 34s are shown in Fig. 4. The average oscillation time is 11s marching the gap between both slug periods. The oscillation extends the period of slug formation. The droplet oscillation does not increase the pressure, however, keeps it horizontal. The upper and lower limits of the oscillation pressures are an average of 111Pa and 83Pa, respectively. The oscillation discharges when the gas pressure reaches 111Pa and closes up by 83Pa. When the gas flow rate rises to 900mL/min corresponding to the $Re_{gas} = 600$, the characteristics of droplet motion are quite different from that discussed above. The droplet is formed at the corner of the channel other than at the water inlet. The little cap droplet thrusts to the corner under high gas flow rate. Several cap droplets form a big droplet, which moves out directly (Fig. S6). The big droplet does not block the channel. The drag force is much stronger than the $P_{detachment}$ pushing the droplet out of the channel. The slug formation can be avoided by feeding with a high Reynolds number. Some residual droplets are seen on the side acrylic wall and the surface of GDL both in both channels. However, as mentioned above, there are some residual droplets only at the vertical corner compared to the arc turning.

The key results from this study are:

1. Gas can bypass the rib and slug and flows through the porous GDL.
2. Water emerges from the largest pore of the hydrophobic GDL into the gas flow channel.
3. The Q_{gas}/D_{bypass} should be 0.13 to eliminate the accumulated water in the channel
4. The minimum gas flow rates should be 10mL/min and 12mL/min in one channel for a single slug and continuous slugs to move out, respectively, at a water flow rate of 10 μ L/min.
5. Channel with a vertical corner can detain some residual droplets. Channel with arc turning is clear under the same conditions. The residual droplets narrow the gas flow channel.
6. The shape of the slug in 1-wall hydrophobic GDL and 3-walls hydrophilic acrylic is similar to an upside-down trapezoid. There is little space at the GDL-acrylic corners which are not filled with liquid.
7. Droplets oscillate when the gas flow rate is higher than 50mL/min in one channel. The oscillation extends the period of slug formation.
8. When the gas flow rate is 900mL/min, the droplets at the water inlet are expelled to the corner, forming a big droplet moving out.

4. CONCLUSION

Four patterns of liquid flow in the micro-channel are received. The order of liquid flow in the channel is; long liquid column formation, slug motion, oscillation, slug motion, and drop motion. The long liquid column almost happened at very low Reynolds numbers while drop motion usually occurs only in high Reynolds numbers. The critical Reynolds number for the transformation liquid flow in the microchannel depends on the parameters in equation 1 and the GDL compression ratios.

Corners in the gas flow channel change the wettability for slug movement. The direction changes in slug motion result in bend loss in the gas flow channel. Additionally, due to the porous GDL materials, slugs at the corner produce the longest bypass distance for gas passing through the GDL and bypassing

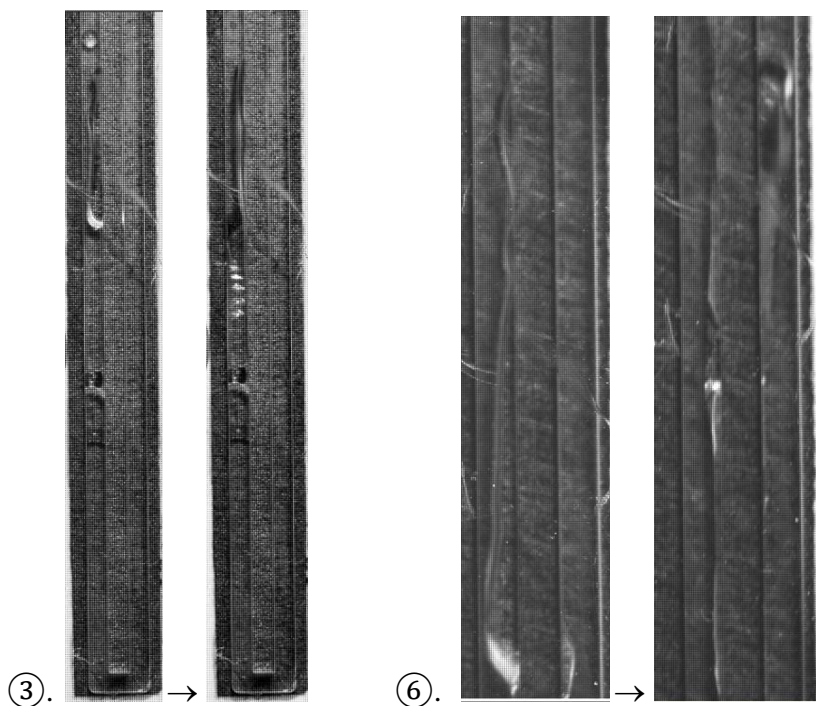
the rib to the adjacent channel. The liquid water stays at corners, resulting in corner-flooding. The corner with arc turning is suitable for slug motion, compared to the corner with sharp turning. The abrupt change in the sharp turning corner transfers the liquid/solid interfacial energy to liquid/vapor interfacial energy.

At a constant GDL compression ratio, increasing the gas flow rates can transfer the liquid flow patterns, facilitating the removal of the liquid water. However, increasing the gas flow rates could result in the oscillation before forming a slug, and extend the period for liquid water removal. Drop motion in high Reynolds number eliminates flooding in fuel cell while causing extra work associated with the gas flow. The gas flow rates are the balances need to integrate consideration of the factors impacting liquid water motion.

ACKNOWLEDGEMENTS

This work was supported by a grant from the National Natural Science Foundation of China (No. 21975192), Foshan Xianhu Laboratory of the Advanced Energy Science and Technology Guangdong Laboratory (XHD2020-002-04).

SUPPORTING INFORMATION:



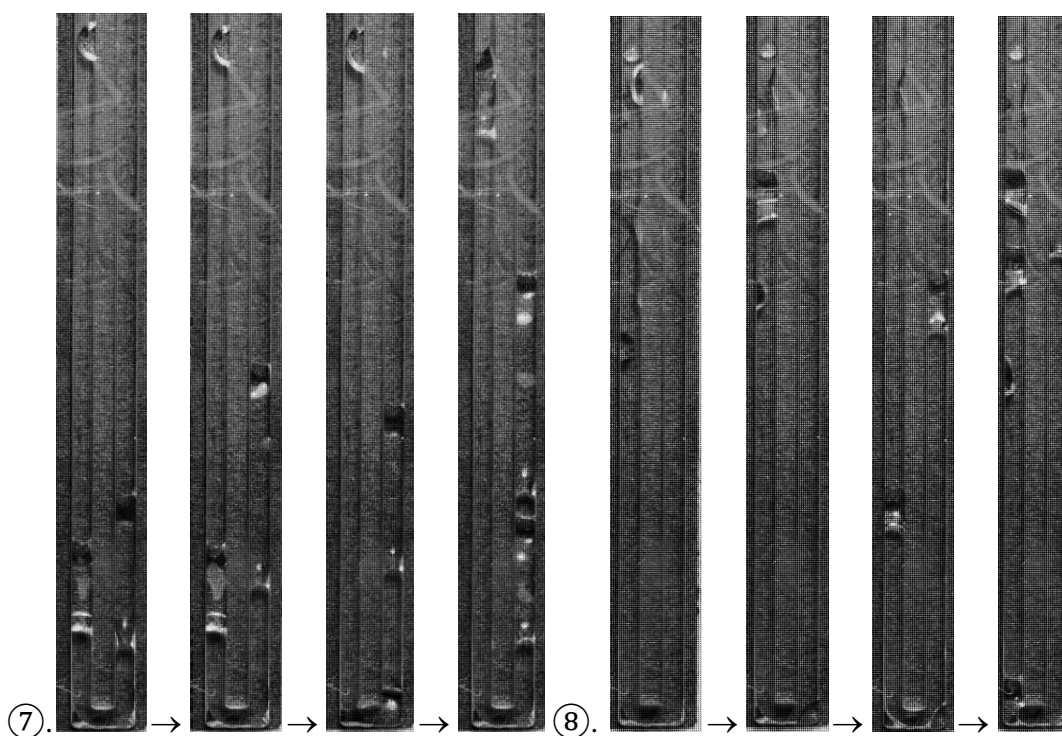


Fig. S1 Regimes of liquid water flow in the microfluidic channel, displaying images corresponding to the definition in Table 1. Some images not shown here, are shown in the following figures.

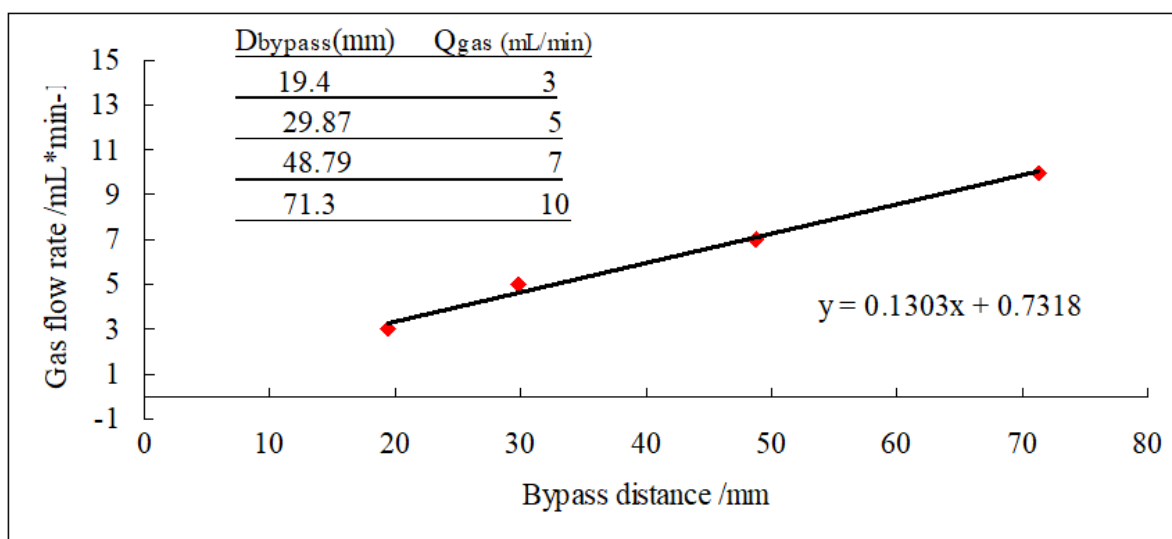


Fig. S2 Gas flow rates as a function of bypass distance for a single slug in the serpentine channel.

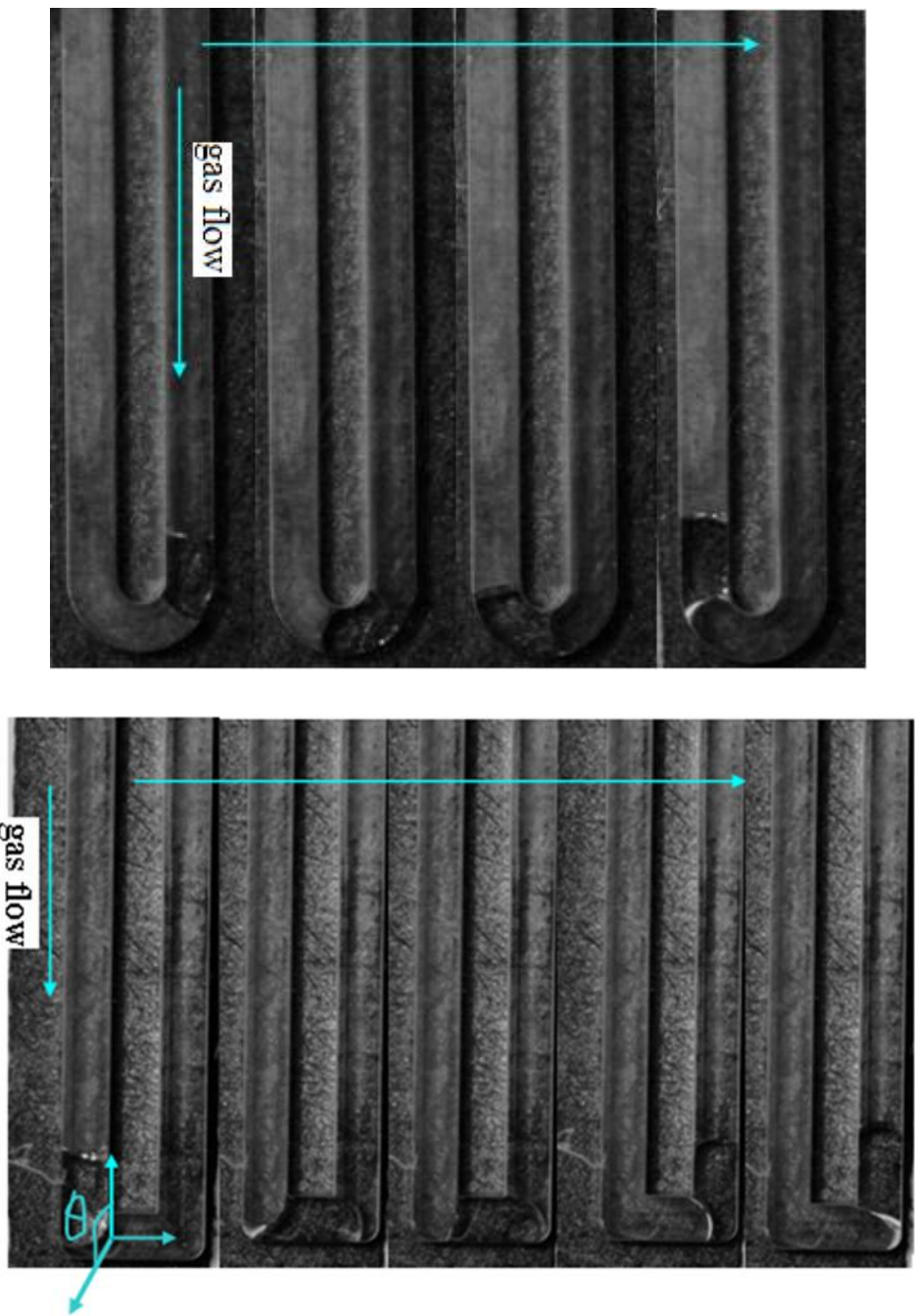


Fig. S3 images for quarter corner and arc corner effects on slug motion.

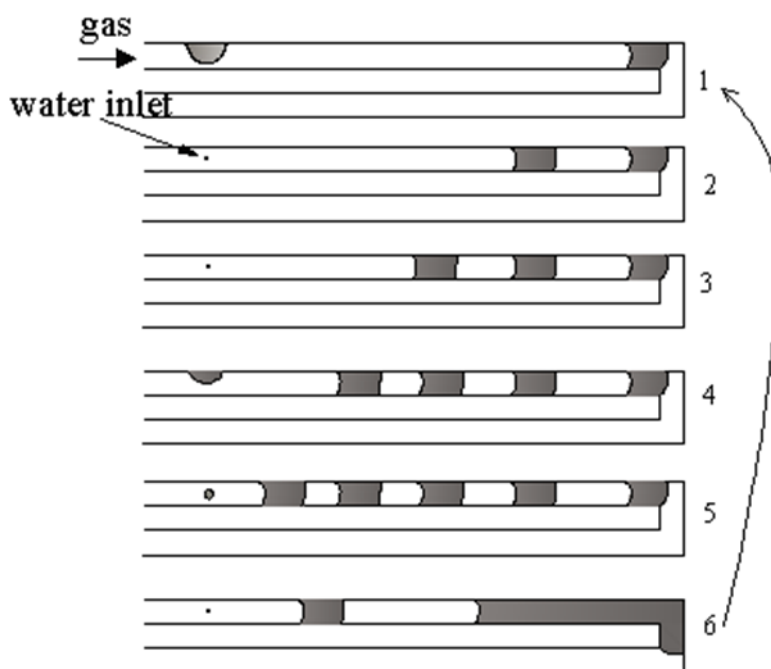


Fig. S4 Continuous slugs motion in the channel with a vertical corner. The gas and water flow rates are 9mL/min and 10 μ L/min, respectively.

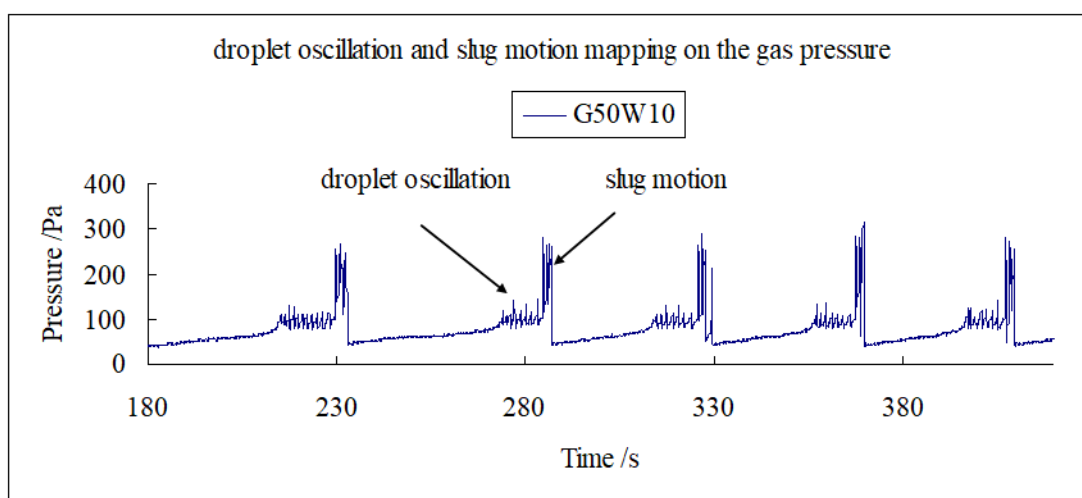


Fig. S5 The in situ pressure trace of droplet oscillation and slug motion.

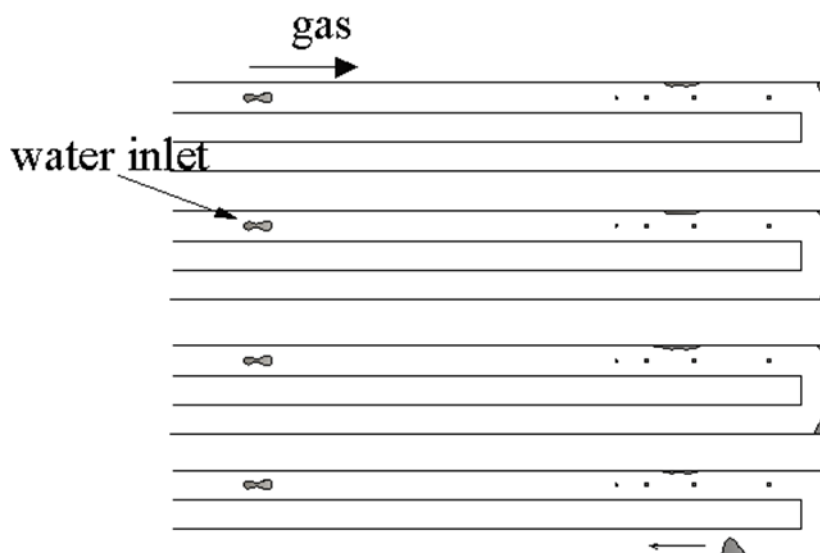


Fig. S6 Droplets motion in high gas flow rate of 900mL/min and water flow rate of 10 μ L/min.

Table S1 Experimental conditions and physical parameters in this study.

Distance from water inlet to the corner	$L = 60mm$
Channel height	$H = 1.6mm$
Channel width	$w_{channel} = 1.6mm$
Rib width	$w_{rib} = 1.6mm$
Pore diameter	$d = 100\mu m$
Gas volumetric flow rate	$Q_{gas} = 3 - 900mL \cdot min^{-1}$
Water volumetric flow rate	$Q_{water} = 10\mu L \cdot min^{-1}$
Gas density	$\rho_{gas} = 1.2kg \cdot m^{-3}$
Gas viscosity	$\mu_{gas} = 1.7 \times 10^{-5} kg \cdot m^{-1} \cdot s^{-1}$
Water viscosity	$\mu_{water} = 1.0 \times 10^{-3} kg \cdot m^{-1} \cdot s^{-1}$
Surface tension of water	$\gamma = 0.072N \cdot m^{-1}$

References

1. S. Rupinder, O.A. Singh, S. Talwinder, *Int. J. Energy Res.*, 46 (2022) 3810-3842.
2. A.R. Kalidindi, R. Taspinar, S. Litster, E.C. Kumbur, *Int. J. Hydrogen Energy*, 38 (2013) 9297-9309.
3. F. Luo, M. Liu, B. Chi, D. Dang, S. Hou, S. Liao, X. Li, H. Song, *J. Appl. Electrochem.*, 48 (2018) 1163-1173.
4. B.H. Lim, E.H. Majlan, W.R.W. Daud, T. Husaini, M.I. Rosli, *J. Ionics*, 22 (2016) 301-316.

5. M. Zago, A. Casalegno, F. Bresciani, R. Marchesi, *Int. J. Hydrogen Energy*, 39 (2014) 21620-21630.
6. P. Polverino, A. Esposito, C. Pianese, *Int. J. Hydrogen Energy*, 38 (2013) 8934-8953.
7. G. Marco, C. Carmine, S. Marco, P. Polverino, P. Cesare, *Appl. Energy*, 279 (2020) 115698.
8. A. Esposito, A. Motello, C. Pianese, Y.G. Guezennec, *Eng. Sci. Technol.*, 7 (2009) 411-420.
9. A. Esposito, C. Pianese, Y.G. Guezennec, *J. Power Sources*, 195 (2010) 4149-4159.
10. P. Željko, B. Christian, B. Frano, S. Joachim, *Energy Convers. Manage.*, 189 (2019) 167-183.
11. K. Inman, X. Wang, *Int. J. Hydrogen Energy*, 39 (2014) 19691-19700.
12. Wang. S, Bi. XT, Wang. SD, *Exp. Therm Fluid Sci.*, 77 (2016) 234-245.
13. E.A. Chinnov, F.V. Ron'shin, O.A. Kabov, *Thermophys. Aeromech.*, 22 (2015) 265-284.
14. C. Xu, Y. Dai, *Ind. Eng. Chem. Res.*, 54 (2015) 6551-6558.
15. K. Kinoshita, E. Parra, A. Hussein, A. Utoft, P. Walke, R. de Bruijn, D. Needham, *J. Processes*, 4 (2016) 2227-9717.
16. J.L. Xu, P. Cheng, T.S. Zhao, *Int. J. Multiphase Flow*, 25 (1999) 411-432.
17. M.S. Nia, P. Oshkai, N. Djilali, *Int. J. Hydrogen Energy*, 44 (2019) 15262-15277.
18. S. Nizetic, F. Barbir, N. Djilali, *Int. J. Hydrogen Energy*, 44 (2019) 9673-9674.
19. S. Hasanpour, M. Ahadi, M. Bahrami, N. Djilali, M. Akbari, *J. Power Sources*, 403 (2018) 192-198.
20. X. Zhu, P.C. Sui, N. Djilali, *Microfluid Nanofluid*, 4 (2008) 543-555.
21. E. Kimball, T. Whitaker, Y.G. Kevrekidis, J.B. Benziger, *Aiche J.*, 54 (2008) 1313-1332.
22. M.J. Cheah, I.G. Kevrekidis, J.B. Benziger, *Langmuir* 29 (2013) 9918-9934.
23. J. Benziger, J.E. Chia, E. Kimball, I.G. Kevrekidis, *J. Electrochem. Soc.*, 154 (2007) B835-B844.
24. W.K. Lee, C.H. Ho, J.W.V. Zee, M. Murthy, *J. Power Sources*, 84 (1999) 45-51.
25. X.M. Han, J.Z. Tan, Y.C. Liu, P. Li, L. Pan, *Int. J. Mech. Mater. Des.*, 750 (2015) 220-225.
26. S.S.L. Rao, A. Shaija, S. Jayaraj, *Mater. Today: Proc.*, 5 (2018) 58-65.
27. Z.Y. Su, C.T. Liu, H.P. Chang, C.H. Li, K.J. Huang, P.C. Sui, *J. Power Sources*, 183 (2008) 182-192.
28. D.K Jiao, K. Jiao, Q. Du, *Int. J. Heat Mass Transfer*, 177 (2021) 0017-9310.
29. T. Hottinen, O. Himanen, S. Karvonen, I. Nitta, *J. Power Sources*, 171 (2007) 113-121.
30. S. Li, B. Sunden, *Int. J. Hydrogen Energy*, 43 (2018) 16279-16292.
31. X.M. Zhang, X.X. Zhang, *Fuel Cells*, 14 (2014) 303-311.
32. T. Hellstern, E. Gauthier, M.J. Cheah, J.B. Benziger, *Int. J. Hydrogen Energy*, 38 (2013) 15414-15427.
33. Z. Lin, X. Peng, X. Wang, *Heat Transfer Asian Res.*, 35 (2006) 13-19.
34. M.J. Cheah, I.G. Kevrekidis, J. Benziger, *J. Phys Chem. B.*, 115 (2011) 10239-10250.
35. E. Gauthier, Q. Duan, T. Hellstern, J. Benziger, *Fuel Cells*, 12 (2012) 835-847.
36. P. Polverino, E. Angelo, P. Cesare, *Int. J. Hydrogen Energy*, 38 (2013) 8934-8953